

Novel Plasma Source for Dense Plasma Effects

D. J. Heading, G. R. Bennett, and J. S. Wark

Department of Physics, Clarendon Laboratory, University of Oxford, Parks Road, Oxford OX1 3PU, United Kingdom

R. W. Lee

Lawrence Livermore National Laboratory, Livermore, California 94551

(Received 22 September 1994)

We describe the production of dense, cool plasmas by the laser ablation of inertially confined foils. Transitions from AlI, AlII, and AlIII ions provide the diagnostic information. The electron density N_e and temperature T_e are $(1-3) \times 10^{19} \text{ cm}^{-3}$ and 1–8 eV, respectively. These conditions are close to those required for complete loss of line features. The fractional depression of the ionization potential for AlI in these plasmas is similar to those found in hot ultradense plasmas.

PACS numbers: 52.50.Jm, 52.25.Jm, 52.25.Rv

The ratio of potential to kinetic energy in a plasma is given by $\Gamma = \langle Z \rangle^2 e / 4\pi \epsilon_0 k_B T R_0$, where R_0 is the ion sphere radius. For a strongly coupled plasma $\Gamma \approx 0.1$ [1,2]. The fundamental physics of dense, cool, strongly coupled plasmas is of interest for a variety of reasons. First, the model for the ionization balance based on a Saha-Boltzmann (SB) equation breaks down as the plasma becomes strongly coupled [3]. Second, significant ionization potential depression (IPD) can occur. Third, there are purely spectroscopic effects in dense, cool plasmas that have long been the subject of study, including significant broadening and shifting of spectral lines; the merging of bound-bound transitions; and the transition from a bound-bound to a bound-free transition [4–6].

These plasma effects are important on an applied level. In the areas of astrophysics [1] and the study of laboratory plasmas created for inertial confinement fusion (ICF) [7,8] there is difficulty in obtaining simple ionization balance models and interpreting spectra. The plasmas described herein give ratios of the IPD to the IP as large as any obtained in the laboratory. Here the time scales are long and the experimental arrangements are more straightforward than in other plasmas where these effects are found. In the most dense ICF implosions reported to date $N_e \geq 10^{24} \text{ cm}^{-3}$ has been measured from a He-like Ar linewidth [7]. Similarly the laser irradiation of solid targets with high-power picosecond pulses has shown that it is possible to achieve $N_e \sim 3 \times 10^{23} \text{ cm}^{-3}$, diagnosed by the IPD of He-like aluminum [9], but again the fractional IPD is larger in the plasmas we discuss here.

Prior to the present experimental work, the spectroscopy of neutral atoms in a plasma had been studied for $N_e \leq 10^{18} \text{ cm}^{-3}$. Calculations presented below indicate that distinct spectral features should persist up to densities $\sim 10^{20} \text{ cm}^{-3}$, where line broadening effects become so large that all the lines are essentially merged. Devices such as flash tubes [10], z pinches [11], and gas-liner pinches [12] can produce dense plasmas. However, radial gradient and opacity effects limit the spectroscopic

usefulness of such sources to $N_e \approx 5 \times 10^{18} \text{ cm}^{-3}$, and T_e from 2–25 eV. Although $N_e > 10^{19} \text{ cm}^{-3}$ have been inferred in capillary plasmas [13], T_e was such (>25 eV) that the predominant ion species produced was triply ionized carbon.

For these reasons the study of neutral atoms in plasmas for N_e approaching 10^{20} cm^{-3} is of specific interest. We report here for the first time a simple method for obtaining dense, cool, quiescent plasmas. The plasmas created are composed of AlI, AlII, and AlIII, have $N_e \geq 10^{19} \text{ cm}^{-3}$, $T_e \sim 1-8$ eV, and persist for a few hundred ns. This is achieved by using confined laser ablation, where the ablating plasma plume is confined to a few hundred micron gap. The primary diagnostic method is time resolved spectroscopy in the range of 400–700 nm.

The experiment was performed using the Vulcan laser at the Central Laser Facility of the Rutherford Appleton Laboratory. The experimental setup is shown in Fig. 1. The target consists of an Al foil held flat by a rear quartz support and separated by $\sim 250 \mu\text{m}$ from a flat 2-mm thick quartz disk. The foil was irradiated through the quartz with up to 3 J of $1.05 \mu\text{m}$ light in a 4.5 ns pulse. The focal spot diameter was 0.7 cm, giving irradiances on target of order 10^9 W cm^{-2} . The absorbed energy was measured to be $\sim 100\%$, in agreement with previous measurements at these irradiances [14].

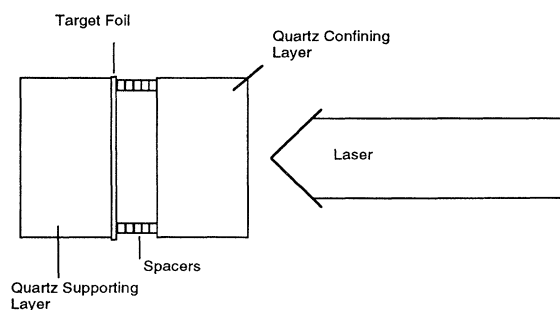


FIG. 1. Target design.

Emission from the plasma, viewed through the quartz wall, was imaged onto the slit of a prism spectrometer, and the dispersed, collimated light incident on the slit of an optical streak camera, at a sweep speed of 5 ns/mm. The time resolved spectrum (400–700 nm) was recorded on a charge coupled device camera. Wavelength, relative intensity calibration, and spectral resolution of the system (0.75 nm HWHM) were measured using combinations of bandpass filters, W and Hg lamps.

The density is determined by three methods. First, using the widths of the spectral lines derived from extrapolations of previously published line data, N_e is determined [4,15]. Second, we assume that the laser energy ablates roughly one skin depth of Al (0.03 μm) which fills the 250 μm gap and yields a density, ρ , of 3.2×10^{-4} g/cm³. This permits an estimate, from an Al equation of state [16], that the peak T_e is ~ 8 eV. This allows the use of an ionization balance model [17] for this T_e and ρ to determine N_e . Third, we compare the entire calculated spectrum produced from our simple model (described below) with the observed spectrum. These estimates yield $N_e \sim (1-3) \times 10^{19}$ cm⁻³.

A typical streaked spectrum is shown in Fig. 2(a). The bright emission in the first 10 ns corresponds to the initial free ablation from the target foil. The subsequent decrease in intensity is due to the adiabatic cooling during expansion into the gap. An increase in emission can be observed ~ 30 ns after the initial free ablation due to the heating of the plasma upon impinging on the confining wall. The ~ 30 ns transit time across the gap is consistent with the velocity of a ~ 8 eV plasma which is similar to the T_e inferred below by spectroscopic means.

Figure 2(b) shows a trace along the spectral direction corresponding to a time 60 ns after the peak of the laser pulse, when uniformity of the plasma will be ensured by hydrodynamic confinement. Visible in the spectrum are the Al II 623 nm [$3s4p-3s^2(S)4d$], and the Al III 452 nm ($4p-4d$) and 570 nm ($4s-4p$) lines. Also shown are the spectra calculated using our model. Figure 2(c) shows the spectrum for a time 130 ns after the laser pulse, and here the Al I 395 nm [$3s^23p-3s^2(^1S)4d$] and Al II 466 nm [$3p^2-3s^2(S)4d$] transitions are seen, together with Al III lines. Calculations are also plotted for three different T_e showing the variation in intensity obtained by varying the T_e for a $N_e = 1.5 \times 10^{19}$ cm⁻³, indicating the sensitivity of the spectra to T_e and confirming the utility of this as a T_e diagnostic.

It can be seen in Fig. 2(a) that the emission lasts for a significant time. Al I and Al II lines are emitted for over 400 ns after the laser pulse. Further, it can be seen from the spectra in Figs. 2(b) and 2(c) that the lines are extremely broad, typically 3–30 nm, corresponding to high electron densities. The difficulty with the absolute wavelength calibration leads to a systematic wavelength error ~ 5 nm. This does not affect the measurement of the linewidths and relative line shifts.

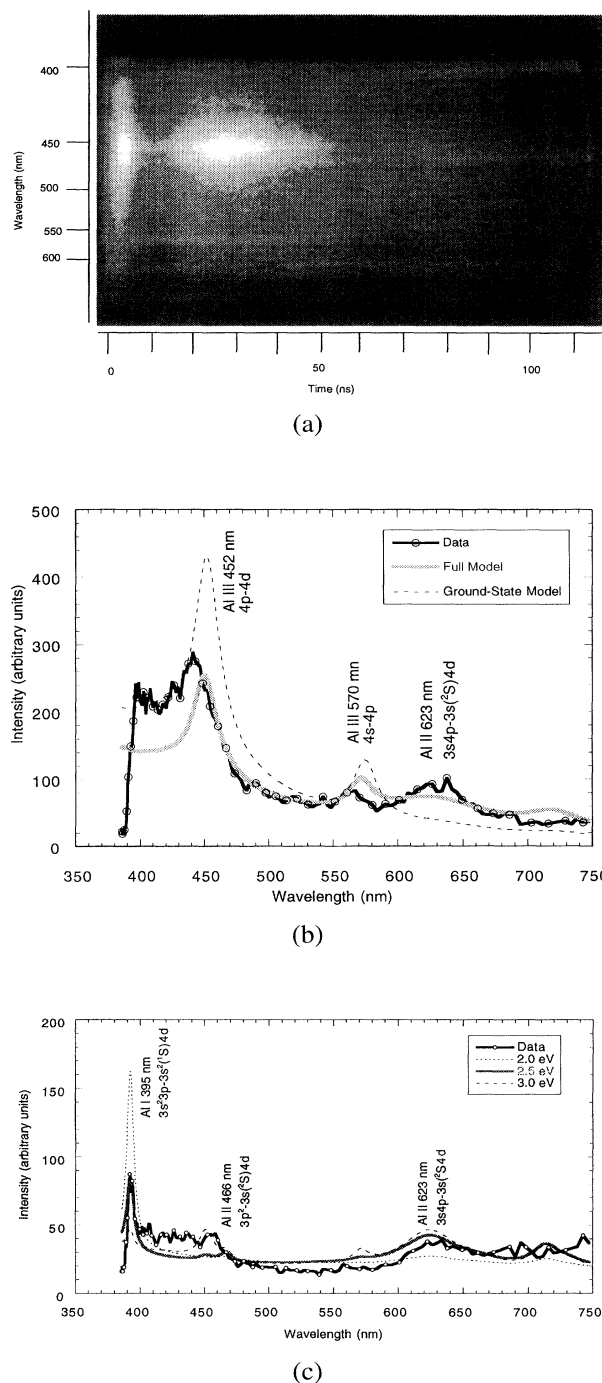


FIG. 2. (a) Experimental streak of a 1.98 J, 4.5 ns FWHM laser pulse, on a target with a 250 μm gap. $t = 0$ corresponds to the start of the laser pulse. (b) Trace from 60 ns after the laser pulse, showing the data obtained and fits to the data using N_e of 2.5×10^{19} cm⁻³ and T_e of 4.3 eV. The thick gray line represents the calculation using excited states to determine the ionization balance while the thin dashed line represents the ground-state-only calculation. (c) Trace from 130 ns after the laser pulse, showing data together with three synthetic spectra obtained for N_e of 1.5×10^{19} cm⁻³, with T_e of 2, 2.5, and 3 eV.

The radial uniformity (<5%) was estimated by space and time resolving the emission through a 7.5-nm band pass filter centered at 535 nm. The effects of thermal losses to the wall on the axial uniformity have been simulated by the use of a 1D Lagrangian hydrocode [18] where the plasma is modeled with the SESAME equation of state and thermal conductivities [16,17]. We find that 60 ns after the laser pulse the temperature is uniform to within 10% over the central 220 μm of the 250 μm gap, and at the edges, next to the confining walls, changes from 90%–10% of its peak value in 3 μm , indicating that the plasma is essentially uniform in this direction. These conclusions are backed up by the experimental observations that we see no line reversal of the Al I resonance line (the optical depth of the center of the Al I resonance line in this boundary layer was calculated as <0.05), no evidence of Si emission until at least 250 ns after the laser pulse, and that the decay time of the inferred temperature is in reasonable agreement with the hydrocode simulations. Furthermore, densities derived from the widths of lines from different ion stages give consistent results.

A simple model was used as a consistency check on N_e and T_e . We assume the plasma to be in local thermodynamic equilibrium (LTE) and optically thin. For $N_e = 10^{19} \text{ cm}^{-3}$, and $T_e = 2 \text{ eV}$, we find, using a hydrogenic approximation [19], that the ion stages of interest are in complete LTE. We calculate an opacity of 0.09 for the Al I 395 nm line (the strongest line observed) at $T_e = 2 \text{ eV}$ and $N_e = 2 \times 10^{19} \text{ cm}^{-3}$. For these conditions $\Gamma \approx 0.2$. This is the limit of the applicability of the Saha-Debye-Huckel theory [3]. To obtain the ion state populations a SB model modified to include the IPD was formulated. This equation of state included partition functions calculated to include the first four manifolds of the ions stages Al I, Al II, Al III, and Al IV, taken from published data [20,21]. States above those explicitly included were treated using a hydrogenic approximation [19]. The inclusion of the excited states was necessary due to the high N_e and low T_e of the plasma. The importance of using a more complete set of states is illustrated in Fig. 2(b) where two calculated spectra are compared to the data. There is a large difference between the spectrum derived from the ionization balance with ground states only compared to both the data and the case including the excited states. Once the ionization fraction had been calculated the spectral position and profile of each line was determined assuming Lorentzian profiles. The linewidth and line shift data produced for use at lower N_e using the semiclassical theory [4,19] and its recent extensions [15,22] have been extrapolated for use here. The effect of the strong coupling on the line shapes is expected to be small [23], and was not included. Electron broadening only is used for the ion profiles, while the Al I width and shift includes ion broadening [4].

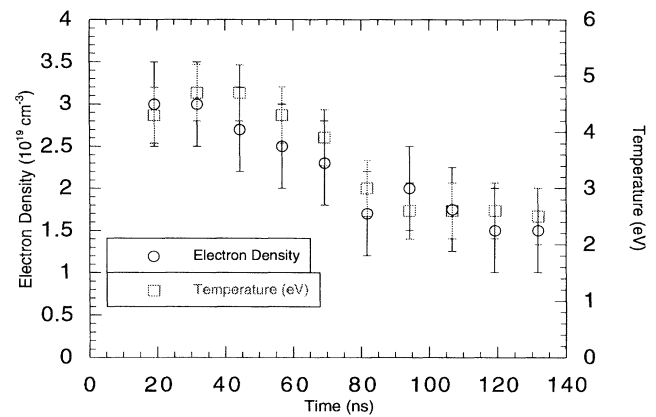


FIG. 3. Time-dependent N_e and T_e derived from fits of calculated spectra to the experimental data.

In Fig. 3 we show the time-dependent N_e and T_e deduced from the comparison between the data and computed spectra. The densities have been inferred from the widths of the Al III 452 nm and Al II 623 nm transitions for the early times with higher T_e and N_e , while the Al II 623 nm and Al I 395 nm transitions are used for later times. The T_e were inferred by determining the spectrum with the closest fit to the observed data, see Fig. 2(c). We estimate the error in T_e to be approximately 0.5 eV. The same analysis provides two diagnostics of N_e , i.e., from the linewidths and the line shift of the Al I 395 nm transition. The shift versus time is shown in Fig. 4 where it is compared to calculated shifts [4] using the diagnosed N_e and T_e . There is reasonable agreement between the calculated and observed shifts. The model results have been independently corroborated by the OPAL code [24].

With our model we can calculate the N_e at which the spectral lines effectively merge into a quasicontinuum.

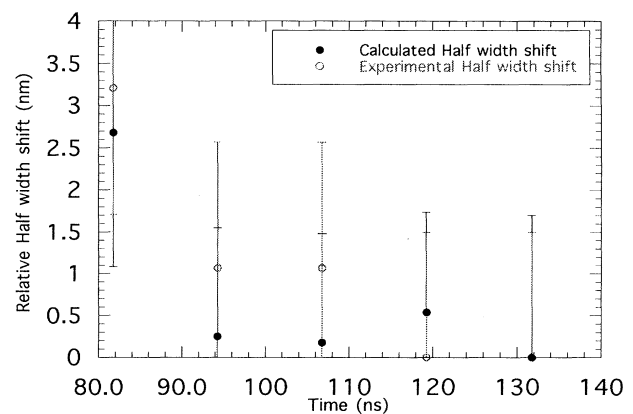


FIG. 4. Relative half-width shifts of the Al I 395 nm [$3s^2 3p-3s^2 (1S) 4d$] line. Zero shift is set at $t = 130 \text{ ns}$.

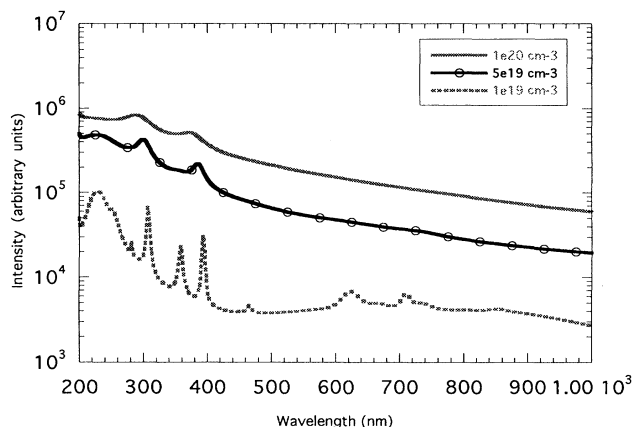


FIG. 5. Calculated spectra at a T_e of 2 eV and N_e of $1 \times 10^{19} \text{ cm}^{-3}$, $5 \times 10^{19} \text{ cm}^{-3}$, and $1 \times 10^{20} \text{ cm}^{-3}$.

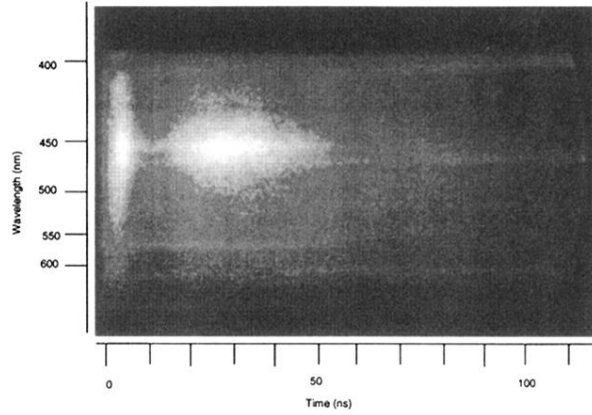
Figure 5 shows that distinct spectral lines merge at $N_e \geq 5 \times 10^{19} \text{ cm}^{-3}$. We note that for the AlI transition at 309 nm to overlap the position of the 395 nm line, $N_e \sim 3 \times 10^{19} \text{ cm}^{-3}$ is required.

In summary, we have shown that a new plasma generation technique can be used to create a uniform plasma in extreme conditions with N_e an order of magnitude higher than previously reported for these low temperatures. Thus, the work reported here is probing the limits of where useful spectroscopy can be performed in the visible region of the spectrum. There are advantages over other forms of laser generated plasmas which are generally small and have very severe gradients, making diagnosis difficult. However, using a less powerful laser with a larger focal spot produces more tractable plasma. It is important to realize that the effects of extreme conditions on the spectroscopy, which has been a constant theme in the generation of these plasmas, may now be studied. As an example one can estimate the IPD as a fraction of the IP and find that we have a reduction of 5% for AlI at $2 \times 10^{19} \text{ cm}^{-3}$ for the plasma presented here, while previous high-power laser plasmas provide, e.g., 4% for He-like Ar at $1 \times 10^{24} \text{ cm}^{-3}$ [7] or He-like Al at $3 \times 10^{23} \text{ cm}^{-3}$ [9]. Therefore, this work constitutes an important advance to the spectroscopy of dense, cool plasma as these data prove we are able to study a new region of T_e , N_e parameter space previously inaccessible.

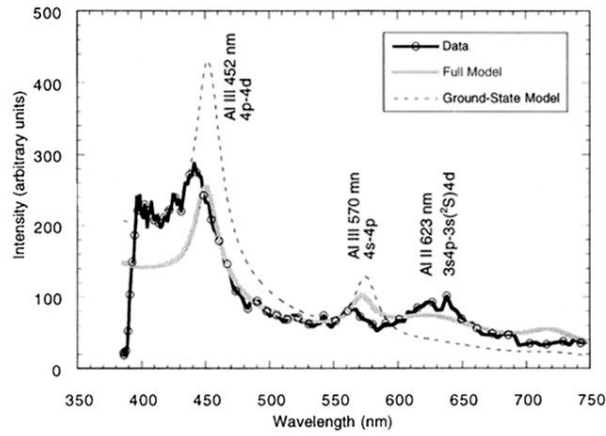
We gratefully acknowledge Dr. F.J. Rogers and Dr. C. A. Iglesias for helpful discussions in connection with

this work, which was supported by the EPSRC under Grant No. GR/H69076.

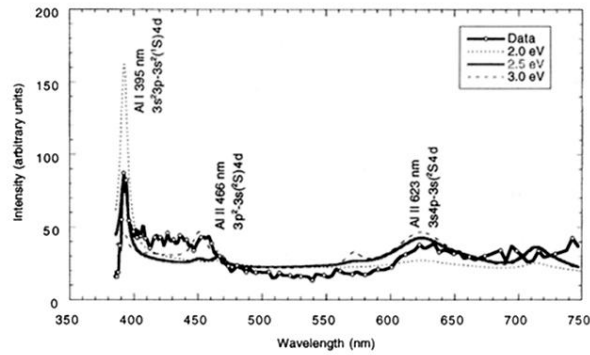
- [1] *Strongly Coupled Plasma Physics*, edited by S. Ichimaru and H.M. Van Horn (University of Rochester Press, Rochester, 1993).
- [2] *Strongly Coupled Plasma Physics*, edited by F.J. Rogers and H.E. DeWitt, NATO ASI, Ser. B, Vol. 154 (Plenum Press, New York, 1987).
- [3] F.J. Rogers, *Phys. Rev. A* **24**, 1531 (1981).
- [4] H.R. Griem, *Spectral Line Broadening By Plasmas* (Academic Press, New York, 1974).
- [5] R.W. Lee, in *Atomic Processes in Plasmas*, edited by E.S. Marmor and J.L. Terry, AIP Conf. Proc. No. 257 (AIP, New York, 1992), p. 39.
- [6] R.W. Lee, *J. Quant. Spectrosc. Radiat. Transfer* **51** (1994).
- [7] B.A. Hammel *et al.*, *Phys. Rev. Lett.* **70**, 1263 (1993).
- [8] C.F. Cooper *et al.*, *Phys. Rev. Lett.* **63**, 267 (1989).
- [9] D. Riley *et al.*, *Phys. Rev. Lett.* **69**, 3739 (1992).
- [10] Y. Vitel, A. Mokhtari, and M. Skowronek, *J. Phys. B* **23**, 651 (1990).
- [11] D.J. Heading, J.P. Marangos, and D.D. Burgess, *J. Phys. B* **25**, 4745 (1992).
- [12] S. Glezner and H.-J. Kunze, *Phys. Rev. E* **49**, 1586 (1994).
- [13] C.A. Morgan, H.R. Griem, and R.C. Elton, *Phys. Rev. E* **49**, 2282 (1994).
- [14] G.R. Bennett *et al.*, *Phys. Rev. E* **50**, 3935 (1994).
- [15] M.S. Dimitrijevic, Z. Djuric, and A.A. Mihajlov, *J. Phys. D* **27**, 247 (1994).
- [16] N.G. Cooper, Los Alamos Scientific Laboratory Report No. LALP-83-4, 1983.
- [17] G.A. Rinker, *Phys. Rev. A* **37**, 1284 (1988).
- [18] J.P. Christiansen, D.E.T.F. Ashby, and K.V. Roberts, *Comput. Phys. Commun.* **7**, 271 (1974).
- [19] H.R. Griem, *Plasma Spectroscopy* (McGraw-Hill, New York, 1964).
- [20] C.E. Moore, *Atomic Energy Levels* (National Bureau of Standards, Washington, 1971), p. 124.
- [21] S. Bashkin and J.O. Stoner, Jr., *Atomic Energy Levels and Grotrian Diagrams I. Hydrogen I-Phosphorous XV* (North-Holland/American Elsevier, New York, 1975), p. 440.
- [22] M.S. Dimitrijevic and S. Sahal-Brechot, *Astron. Astrophys. Suppl. Ser.* **99**, 585 (1993).
- [23] D.B. Boercker, R.W. Lee, and F.J. Rogers, *J. Phys. B* **16**, 3279 (1983).
- [24] C.A. Iglesias and F.J. Rogers (private communication).



(a)



(b)



(c)

FIG. 2. (a) Experimental streak of a 1.98 J, 4.5 ns FWHM laser pulse, on a target with a $250 \mu\text{m}$ gap. $t = 0$ corresponds to the start of the laser pulse. (b) Trace from 60 ns after the laser pulse, showing the data obtained and fits to the data using N_e of $2.5 \times 10^{19} \text{ cm}^{-3}$ and T_e of 4.3 eV. The thick gray line represents the calculation using excited states to determine the ionization balance while the thin dashed line represents the ground-state-only calculation. (c) Trace from 130 ns after the laser pulse, showing data together with three synthetic spectra obtained for N_e of $1.5 \times 10^{19} \text{ cm}^{-3}$, with T_e of 2, 2.5, and 3 eV.